

Chapter 5

Direct Torque Control using Matrix Converters

The Direct Torque Control (DTC) is a high-dynamic and high performance control technique for induction motor drives which has been developed in the last two decades [1]-[8] as possible alternative solution to DC servo drives.

In direct-torque-controlled adjustable speed drives the motor flux and the electromagnetic torque are the reference quantities which are directly controlled by the applied inverter voltage vector. At any cycle period, accordingly to the position of the motor flux space vector and the output signals of a flux and a torque hysteresis comparators the most opportune inverter switching state is selected.

The main advantages of the basic DTC scheme are:

- the simplicity, as no coordinate transformation is required;
- the high dynamic;
- the robustness;
- the sensorless operation;

DTC has also some disadvantages, as the difficulty to control the torque and the flux at very low speed, the higher current and torque ripple which imply higher machine losses and noise, the inherent variable switching frequency, the lack of direct current control.

A general block diagram of DTC scheme is represented in Fig. 1.

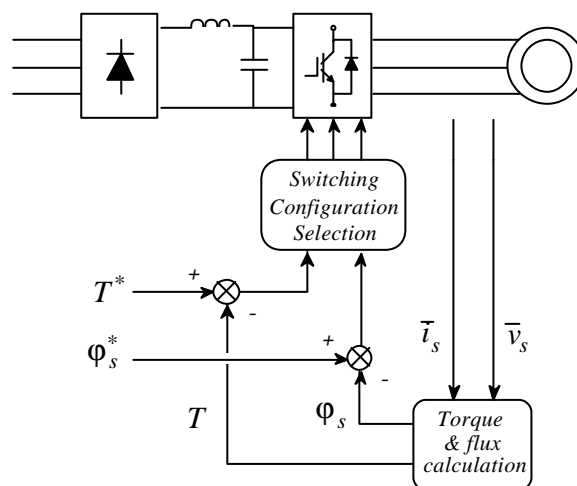


Fig.5.1 Basic DTC block diagram.

It is evident by the diode rectifier that the AC drive shown in Fig.5.1 does not have bidirectional energy flow capability. This limit might be overcome by a traditional inverter back-to-back arrangement but it might be also solved in a more elegant and effective way by using a matrix converter. The matrix converter would allow, in addition to a straight-forward bidirectional energy flow, sinusoidal input currents and the control capability of the input power factor, as consequence of its higher number of switching state configurations compared to traditional voltage source inverter (VSI).

In this chapter, after a short introduction to the direct torque control scheme of induction machines, it is presented a control method for matrix converters which allows, under the constraint of unity input power factor, the generation of the voltage vectors required to implement DTC [9].

The performance of the proposed control method are analyzed and discussed on the basis of realistic numerical simulations as well as experimental tests of the whole drive system [10]. The control method has been implemented on a matrix converter adjustable speed drive prototype with the Institute of Energy Technology at the University of Aalborg, Denmark.

5.1. Direct Torque Control of induction machines

The DTC technique was firstly proposed by Takahashi [1] as a new quick-torque-response and high efficiency control strategy for induction motor. This technique allows to independently control the motor flux, which can be the stator, the rotor or the magnetizing flux, and the electromagnetic torque, at the same time.

If the stator flux is assumed as reference, the estimated values of flux and torque can be calculated just taking into account the stator currents and voltages. Furthermore, the stator resistance is the only motor parameter needed [11]. This is a feature which significantly contributes to the DTC scheme robustness.

The torque control is achieved by quickly changing the position of the stator flux space vector $\bar{\varphi}_s$ with respect to the rotor flux space vector $\bar{\varphi}_r$. In fact, for a symmetrical three-phase induction machine, the electromagnetic torque T_{em} is proportional to the scalar product of the stator flux vector $\bar{\varphi}_s$ and the rotor flux vector $\bar{\varphi}_r$, referred to a stationary stator reference frame. The following relation holds:

$$T_{em} = \frac{3}{2} p A \left[\bar{\varphi}_s \cdot j \bar{\varphi}_r \right] \quad \text{with} \quad A = \frac{M}{L_S L_R - M^2} \quad (5.1)$$

where L_S is the stator self-inductance coefficient, L_R is the rotor self-inductance coefficient in a stator reference frame, M is the mutual inductance coefficient and p the number of poles pairs.

Now, it can be demonstrated that the stator and rotor flux vectors $\bar{\varphi}_s$ and $\bar{\varphi}_r$ are related by the following expression

$$\dot{\bar{\varphi}}_r B + \bar{\varphi}_r (1 - j B \omega_m) = \frac{M}{L_S} \bar{\varphi}_s \quad \text{with} \quad B = \left(L_R - \frac{M^2}{L_S} \right) \frac{1}{R_R} \quad (5.2)$$

where $\dot{\bar{\varphi}}_r$ is the time derivative of the rotor flux space vector, R_R is the rotor resistance in the stator frame and ω_m is the mechanical angular velocity of the rotor.

Equation (5.2) shows that there is a low-pass filter relation between $\bar{\varphi}_s$ and $\bar{\varphi}_r$. This means that the rotor flux vector follows the stator flux vector variations with a finite time delay. The DTC capability to have rapid instantaneous torque variations is based right on this time delay.

The control quantities through which the DTC tracks the reference flux and torque are the radial $D\bar{\varphi}_{sr}$ and the tangential $D\bar{\varphi}_{st}$ components of the stator flux variation $D\bar{\varphi}_s$ impressed by the inverter voltage vector applied to the motor. The expression of the stator flux vector variation $D\bar{\varphi}_s$ in terms of its radial and tangential components is given by

$$D\bar{\varphi}_s = D\bar{\varphi}_{sr} + D\bar{\varphi}_{st} = D\varphi_{sr} \hat{r} + D\varphi_{st} \hat{t} \quad (5.3)$$

As it can be sensed by Fig.5.2, the radial component controls the stator flux vector amplitude while the tangential component controls the stator flux vector angular position and hence the torque.

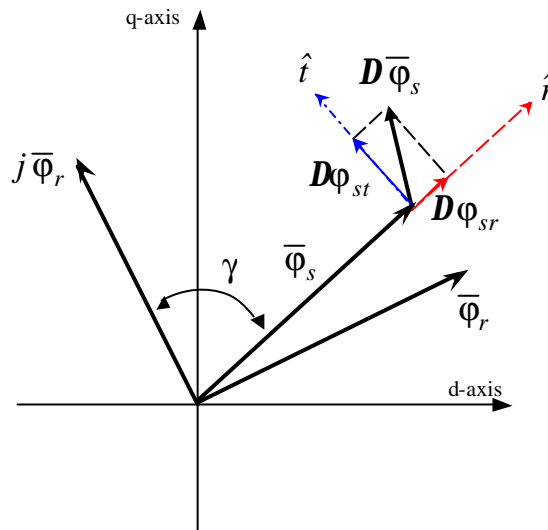


Fig.5.2 Representation of the torque generation operating principle.

The stator flux vector variation $D\bar{\varphi}_s$ is resolved in its radial

$D\bar{\varphi}_{sr}$ and tangential $D\bar{\varphi}_{st}$ vector components.

In Fig.5.3 the schematic circuit of a voltage source inverter is represented along with the voltage vectors corresponding to the eight different switching configurations that it can assume. Two of them determine zero voltage vectors, \bar{v}_0 and \bar{v}_7 , while the remaining generate six equally

spaced voltage vectors having the same magnitude. Equation (5.4) gives the general expression for a VSI voltage vector, where U_{DC} is the DC link voltage.

In Fig.5.3 it is also shown how the d-q stator reference frame is divided in sectors.

$$\bar{v}_k = \frac{2}{3} U_{DC} e^{j(k-1)\frac{\pi}{3}} \quad k = 1, 2, \dots, 6 \quad (5.4)$$

Now, for the induction motor stator winding the following equation in terms of space vectors can be written with reference to a stator frame:

$$\bar{v}_s = R_s \bar{i}_s + \frac{d\bar{\phi}_s}{dt} \quad (5.5)$$

where \bar{v}_s and \bar{i}_s are the stator voltage and current space vectors respectively. If it is assumed, for simplicity, to neglect the voltage drop on the stator resistance R_s and to consider a short finite time Δt , representing the control cycle period, equation (5.5) reduces to the following equation

$$\Delta\bar{\phi}_s = \bar{v}_s \Delta t \quad (5.6)$$

Some remarks can be made with regard to equation (5.6).

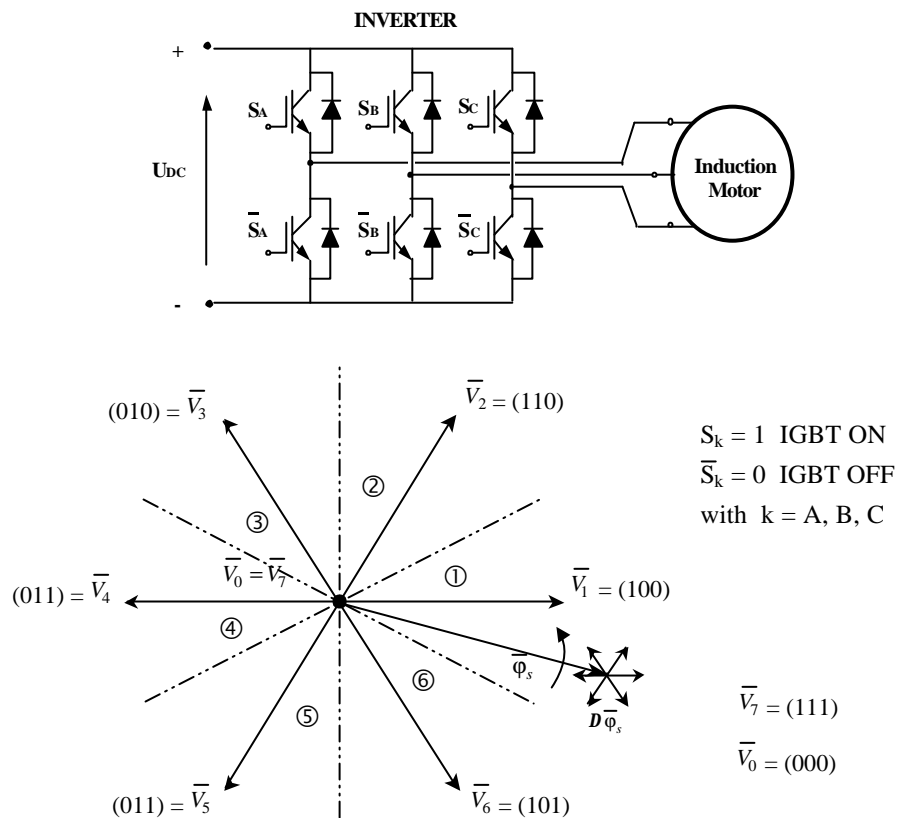


Fig.5.3 Schematic circuit of a voltage source inverter and relevant switching configurations voltage vectors

First, it shows that the applied inverter voltage vector, $\bar{v}_k = \bar{v}_s$, directly impresses the stator flux space vector. This means that the required stator flux vector locus will be obtained by using the opportune inverter output voltage vectors and hence inverter configurations.

Second, equation (5.6) shows that the stator flux space vector moves by the discrete amount $D\bar{\varphi}_s$ in the direction of the voltage vector applied by the inverter. The amplitude of the variation depends on the DC link voltage, by way of equation (5.4). For a given DC link voltage level, setting the control cycle period Δt the minimum stator flux vector variation $D\bar{\varphi}_s$ is defined.

Substituting equation (5.6) in equation (5.3) the following is obtained

$$D\varphi_{sr} \hat{r} + D\varphi_{st} \hat{t} = \bar{v}_s D t = (v_{sr} \hat{r} + v_{st} \hat{t}) D t \quad (5.7)$$

Equation (5.7) explicitly states that the decoupled control of the stator flux and the electromagnetic torque can be carried out by way of the selection of the opportune inverter voltage vector, and hence switching configuration.

It is worth noting that due to the fixed direction of the inverter voltage vectors and to the rotating motion of the stator flux vector $\bar{\varphi}_s$ in the d-q stator frame, for each inverter voltage vector the amplitude of its radial and tangential components will be variable within a sector.

At each cycle period, hereinafter indicated by t_C , the selection of the proper inverter voltage vector is made in order to maintain the estimated torque and stator flux within the limits of two hysteresis bands. More precisely, the vector choice is made on the basis of the position of the stator flux vector and the instantaneous errors in torque and stator flux magnitude.

As an example, considering the stator flux vector laying in sector ①, as shown in Fig.5.3, the voltage vectors \bar{V}_2 and \bar{V}_6 can be selected in order to increase the flux while \bar{V}_3 and \bar{V}_5 can be applied to decrease the flux. Among these, \bar{V}_2 and \bar{V}_3 determine a torque increase, while \bar{V}_5 and \bar{V}_6 a torque decrease. The zero voltage vectors are selected when the output of the torque comparator is zero, irrespective to the stator flux condition. Using the basic switching table given in Table I it is possible to implement DTC scheme having good performance.

Table I
Basic DTC inverter configuration selection table.

Sector of $\bar{\varphi}_s$	$C_\varphi = -1$			$C_\varphi = 1$		
	$C_T = -1$	$C_T = 0$	$C_T = 1$	$C_T = -1$	$C_T = 0$	$C_T = 1$
①	V_2	V_7	V_6	V_3	V_0	V_5
②	V_3	V_0	V_1	V_4	V_7	V_6
③	V_4	V_7	V_2	V_5	V_0	V_1
④	V_5	V_0	V_3	V_6	V_7	V_2
⑤	V_6	V_7	V_4	V_1	V_0	V_3
⑥	V_1	V_0	V_5	V_2	V_7	V_4

It should be noted that Table I is not the only possible DTC switching table. In general, modified switching table have been proposed in literature with the intention to improve the performance of the DTC scheme at very low and very high rotor speed [3], [7].

5.2. Matrix Converter space vector representation

The proposed control method relies on a space vector representation of the matrix converter switching configurations. As for the SVM modulation strategies presented in chapter 4, this control method make use of the active and zero configurations only, which are quoted in Table II. It has to be highlighted that with respect to Table I of chapter 4, in Table II the output line-to-neutral voltage space vector \bar{e}_o is considered.

Table II
Switching configurations of the matrix converter used in the proposed DTC control scheme.

Switching Configuration	A B C	v_{AB}	v_{BC}	v_{CA}	i_a	i_b	i_c	e_o	a_o	i_i	b_i
+1	<i>a b b</i>	v_{ab}	0	$-v_{ab}$	i_A	$-i_A$	0	$2/3 v_{ab}$	0	$2/\sqrt{3} i_A$	$-p/6$
-1	<i>b a a</i>	$-v_{ab}$	0	v_{ab}	$-i_A$	i_A	0	$-2/3 v_{ab}$	0	$-2/\sqrt{3} i_A$	$-p/6$
+2	<i>b c c</i>	v_{bc}	0	$-v_{bc}$	0	i_A	$-i_A$	$2/3 v_{bc}$	0	$2/\sqrt{3} i_A$	$p/2$
-2	<i>c b b</i>	$-v_{bc}$	0	v_{bc}	0	$-i_A$	i_A	$-2/3 v_{bc}$	0	$-2/\sqrt{3} i_A$	$p/2$
+3	<i>c a a</i>	v_{ca}	0	$-v_{ca}$	$-i_A$	0	i_A	$2/3 v_{ca}$	0	$2/\sqrt{3} i_A$	$7p/6$
-3	<i>a c c</i>	$-v_{ca}$	0	v_{ca}	i_A	0	$-i_A$	$-2/3 v_{ca}$	0	$-2/\sqrt{3} i_A$	$7p/6$
+4	<i>b a b</i>	$-v_{ab}$	v_{ab}	0	i_B	$-i_B$	0	$2/3 v_{ab}$	$2p/3$	$2/\sqrt{3} i_B$	$-p/6$
-4	<i>a b a</i>	v_{ab}	$-v_{ab}$	0	$-i_B$	i_B	0	$-2/3 v_{ab}$	$2p/3$	$-2/\sqrt{3} i_B$	$-p/6$
+5	<i>c b c</i>	$-v_{bc}$	v_{bc}	0	0	i_B	$-i_B$	$2/3 v_{bc}$	$2p/3$	$2/\sqrt{3} i_B$	$p/2$
-5	<i>b c b</i>	v_{bc}	$-v_{bc}$	0	0	$-i_B$	i_B	$-2/3 v_{bc}$	$2p/3$	$-2/\sqrt{3} i_B$	$p/2$
+6	<i>a c a</i>	$-v_{ca}$	v_{ca}	0	$-i_B$	0	i_B	$2/3 v_{ca}$	$2p/3$	$2/\sqrt{3} i_B$	$7p/6$
-6	<i>c a c</i>	v_{ca}	$-v_{ca}$	0	i_B	0	$-i_B$	$-2/3 v_{ca}$	$2p/3$	$-2/\sqrt{3} i_B$	$7p/6$
+7	<i>b b a</i>	0	$-v_{ab}$	v_{ab}	i_C	$-i_C$	0	$2/3 v_{ab}$	$4p/3$	$2/\sqrt{3} i_C$	$-p/6$
-7	<i>a a b</i>	0	v_{ab}	$-v_{ab}$	$-i_C$	i_C	0	$-2/3 v_{ab}$	$4p/3$	$-2/\sqrt{3} i_C$	$-p/6$
+8	<i>c c b</i>	0	$-v_{bc}$	v_{bc}	0	i_C	$-i_C$	$2/3 v_{bc}$	$4p/3$	$2/\sqrt{3} i_C$	$p/2$
-8	<i>b b c</i>	0	v_{bc}	$-v_{bc}$	0	$-i_C$	i_C	$-2/3 v_{bc}$	$4p/3$	$-2/\sqrt{3} i_C$	$p/2$
+9	<i>a a c</i>	0	$-v_{ca}$	v_{ca}	$-i_C$	0	i_C	$2/3 v_{ca}$	$4p/3$	$2/\sqrt{3} i_C$	$7p/6$
-9	<i>c c a</i>	0	v_{ca}	$-v_{ca}$	i_C	0	$-i_C$	$-2/3 v_{ca}$	$4p/3$	$-2/\sqrt{3} i_C$	$7p/6$
0 _a	<i>a a a</i>	0	0	0	0	0	0	0	--	0	--
0 _b	<i>b b b</i>	0	0	0	0	0	0	0	--	0	--
0 _c	<i>c c c</i>	0	0	0	0	0	0	0	--	0	--

For the output line-to-neutral voltage vector \bar{e}_o and the matrix converter input current vector \bar{i}_i the following expressions hold.

$$\bar{e}_o = \frac{2}{3} \left(e_{oA} + e_{oB} e^{j2\pi/3} + e_{oC} e^{j4\pi/3} \right) = e_o(t) e^{j\alpha_o(t)} \quad (5.8)$$

$$\bar{i}_i = \frac{2}{3} \left(i_{ia} + i_{ib} e^{j2\pi/3} + i_{ic} e^{j4\pi/3} \right) = i_i(t) e^{j\beta_i(t)} \quad (5.9)$$

In Figs.5.4 and 5.5 the output line-to-neutral voltage and the input current vectors for the active configurations are respectively shown.

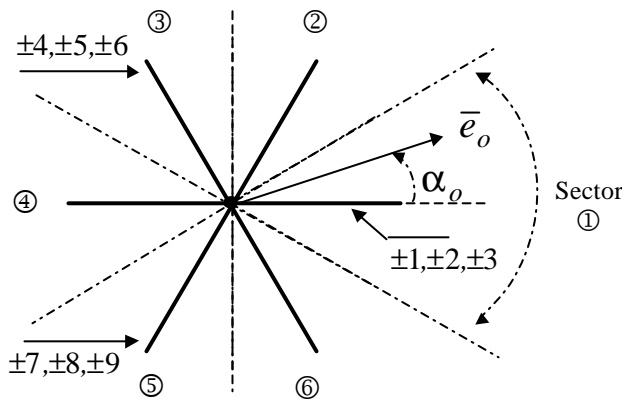


Fig.5.4 Output voltage vectors for active configurations and reference output voltage vector.

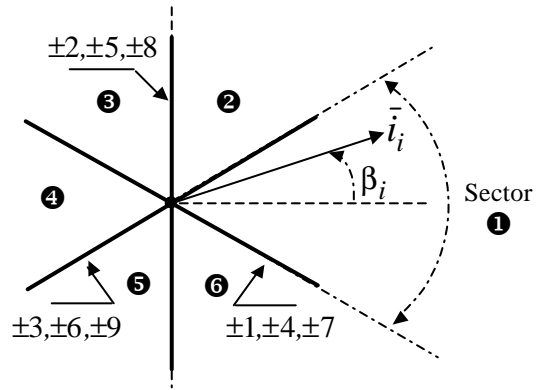


Fig.5.5 Input current vectors for active configurations and reference input current vector.

5.3 The use of matrix converter in DTC

In the same way as for matrix converter space vector modulated control method, the reference control quantities are the output voltage vector and the input current vector phase displacement with respect to the input line-to-neutral voltage vector. But the choice of the switching configuration to apply is made on a totally different basis.

The control of the output voltage is based on the classical DTC scheme described in section 5.1. As a consequence, at each cycle period the optimum vector, among the eight generated by a VSI, is selected in switching Table I accordingly to the position of the stator flux vector and the output signals C_ϕ and C_T of the stator flux and torque hysteresis comparators. In Figs.5.6 and 5.7 the two-level stator flux and the three-level electromagnetic torque hysteresis comparators are respectively shown.

Once the classical DTC control scheme has selected the optimum vector to be applied to the machine, it is a matter of determining the correspondent matrix converter switching configuration. If it is assume, for example, that the VSI output vector \bar{V}_1 has been chosen,

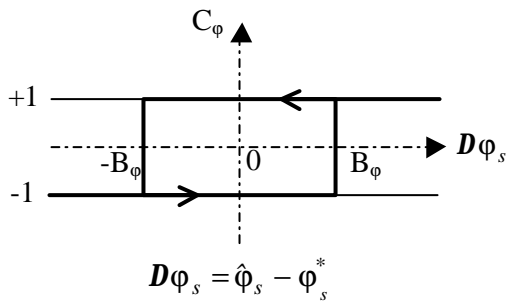


Fig.5.6 Two-level stator flux hysteresis comparator.

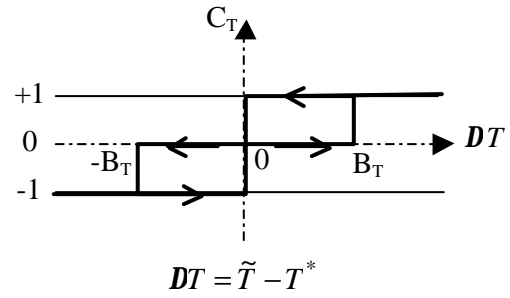


Fig.5.7 Three-level torque hysteresis comparator.

looking at Table II and Figs.5.3 and 5.4, it can be seen that matrix converter can generate the same vector by means of the switching configurations $\pm 1, \pm 2, \pm 3$. But not all of them can be usefully employed to provide vector \bar{V}_1 .

In fact, at any instant, the magnitude and the direction of their corresponding output voltage vectors depend on the position of the input line-to-neutral voltage vector \bar{e}_i . Among the 6 vectors, those having the same direction of \bar{V}_1 and the maximum magnitude are considered.

If it is assume, for example, that vector \bar{e}_i is in sector ①, the switching configurations to be used are +1 and -3. In fact, looking at Fig.5.8 and Table II it can be seen that within sector ① these two switching configurations are those which complies with the above mentioned selection criteria.

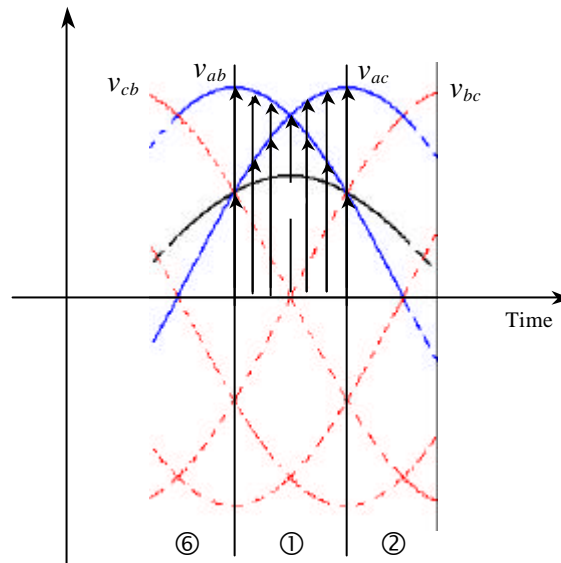


Fig.5.8 Representation of the input line-to-line voltages in the time domain for sector ① of the input line-to-neutral voltage vector

It has been verified that, whatever is the sector which the vector \bar{e}_i is in, the matrix converter makes always available two switching configurations for each VSI output vector chosen by the classical DTC scheme.

Such redundancy gives the opportunity to control a further variable in addition to the stator flux and the electromagnetic torque.

In the proposed control method the average value of the sine of the displacement angle ψ_i between the input current vector and the corresponding input line-to-neutral voltage vector has been chosen as third variable. This variable will be indicated by $\langle \sin \psi_i \rangle$.

If the constraint to comply with is an unity input power factor, such aim can be achieved keeping the value of $\langle \sin \psi_i \rangle$ to zero. The variable $\langle \sin \psi_i \rangle$ is directly controlled by the hysteresis comparator shown in Fig.5.9. The average value of $\sin \psi_i$ is obtained applying a low-pass filter to its instantaneous estimated value.

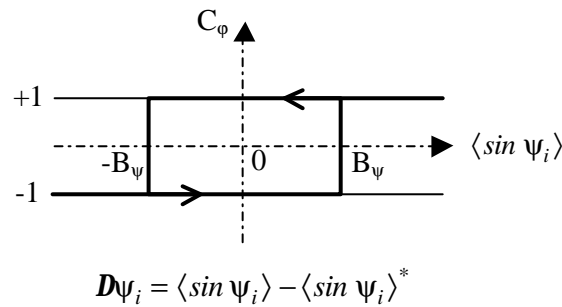


Fig.5.9 Hysteresis comparator of the $\langle \sin \psi_i \rangle$ value.

The control of the input power factor is possible because the input current vector for switching configurations +1 and -3 have different directions, as it can be seen from Table II and shown in Fig.5.10.

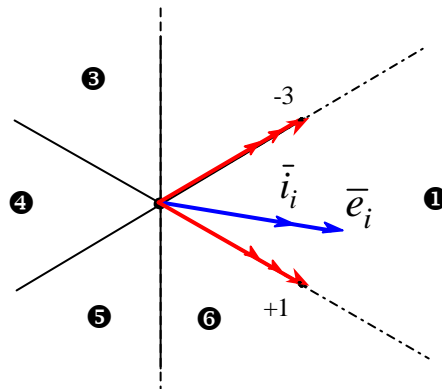


Fig.5.10 Representation of an unity control of the input power factor.

Keep going with the previous example, it is assumed by Fig.5.10 that the reference input displacement angle is set to zero. As a consequence the reference value of $\langle \sin \psi_i \rangle$ is also set to zero, $\langle \sin \psi_i \rangle^* = 0$.

Now, if the estimated value of $\langle \sin \psi_i \rangle$ is positive, $C_\varphi = +1$, which means that the input current vector \bar{i}_i is lagging the voltage vector \bar{e}_i , then the configuration -3 has to be applied.

On the contrary, if the estimated value of $\langle \sin \psi_i \rangle$ is negative, $C_\psi = -1$, which means that the input current vector \bar{i}_i is leading the voltage vector \bar{e}_i , the configuration +1 has to be applied.

The switching table based on these principles is shown in Table III.

Table III
Matrix Converter Switching Table for DTC control.

	1		2		3		4		5		6	
C_ψ	+1	-1	+1	-1	+1	-1	+1	-1	+1	-1	+1	-1
V_1	-3	1	2	-3	-1	2	3	-1	-2	3	1	-2
V_2	9	-7	-8	9	7	-8	-9	7	8	-9	-7	8
V_3	-6	4	5	-6	-4	5	6	-4	-5	6	4	-5
V_4	3	-1	-2	3	1	-2	-3	1	2	-3	-1	2
V_5	-9	7	8	-9	-7	8	9	-7	-8	9	7	-8
V_6	6	-4	-5	6	4	-5	-6	4	5	-6	-4	5

The first column on the left hand side contains the voltage vectors selected by the basic DTC scheme in order to keep the stator flux and torque within the limits of the corresponding hysteresis bands.

The other six bold columns, are related to the sector of the matrix converter input current vector \bar{i}_i . Depending on the output value of the C_ψ hysteresis comparator, the left or the right column has to be used in selecting the switching configuration of the matrix converter.

When a zero voltage vector is required from Table I, the zero configuration of the matrix converter which minimizes the number of commutations is selected.

The output of the hysteresis regulator C_ψ , together with the sector number of the input current vector and the voltage vector required by the DTC, are the input to the matrix converter switching configuration selection algorithm represented by Table III.

It is worth noting that in [19] the sectors were related the input line-to-neutral voltage vector \bar{e}_i . The matrix converter switching configurations selected on the basis of the \bar{e}_i or \bar{i}_i vectors sector are identical only in the case of unity input power factor. In the case of an input power factor different from unity, for a proper control of the matrix converter input current, the switching configuration selection has to be referred to the sector of the \bar{i}_i vector.

But likewise to the space vector modulated matrix converter, if the input power factor is controlled to be less than unity, a reduction in the voltage transfer ratio is the result, which in the DTC application turns into a reduction of the dynamic performance of the drive. In Fig.5.11 it is shown the block diagram of the proposed DTC control scheme for the matrix converter.

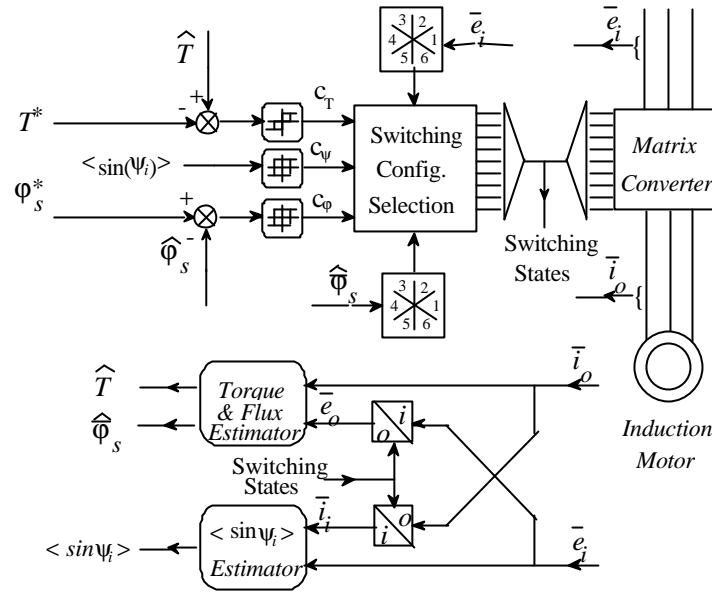


Fig.5.11 Block diagram of the proposed DTC scheme for matrix converter.

With reference to Fig.5.11, in the lower part of the diagram the estimators of the electromagnetic torque, the stator flux and the average value of $\sin \psi_i$ are represented. It is evident that these estimators require the knowledge of input and output voltages and currents. However, only the input voltages and the output currents are measured in each cycle period, because the other quantities can be calculated on the basis of the actual switching configuration of the matrix converter which is known.

5.4 Numerical simulations and experimental tests of a Matrix-DTC drive system

In order to verify the feasibility of this drive system and its performance, a numerical analysis has been firstly carried out using the mathematical model of a simplified matrix converter drive system, whose schematic circuit is shown in Fig.5.12.

The results obtained by the analysis [9], demonstrated the feasibility of the DTC control scheme as well as its good performance. In Figs.5.13-5.16 some results are shown. The simulations were carried out assuming a cycle period of $40 \mu\text{s}$ and ideal switching devices. Phenomena like the influence of discretization and the delay caused by the sampling of signals were also taken into account.

The test machine was a standard 4 kW, 4-pole, 220 V, 50 Hz cage induction motor having the following parameters:

$$R_S = 0,51 \Omega \quad R_R = 0,42 \Omega \quad L_S = 58.2 \text{ mH} \quad L_R = 58.2 \text{ mH} \quad M = 56 \text{ mH}$$

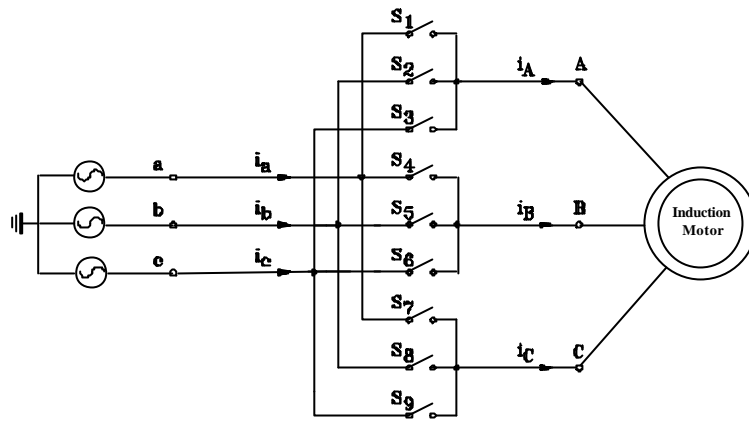


Fig.5.12 Schematic circuit of the simplified matrix converter DTC drive.

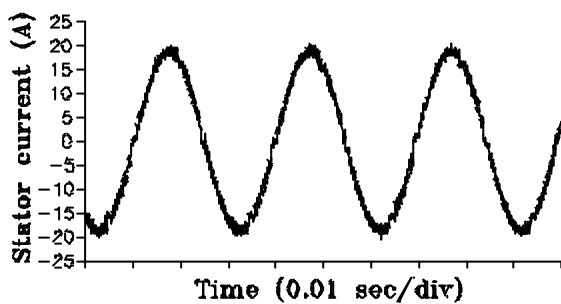


Fig.5.13 Stator current at 1000 rpm, 25 Nm. (reprinted from [9], Fig.9, pp.747)

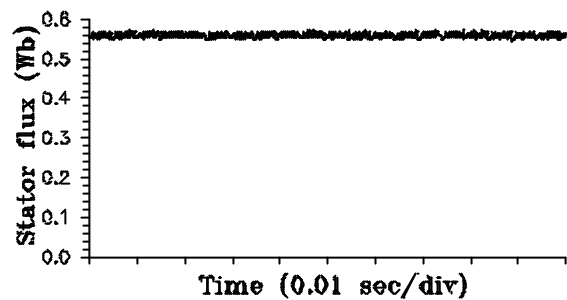


Fig.5.14 Stator flux magnitude at 1000 rpm, 25 Nm. (reprinted from [9], Fig.10, pp.747)

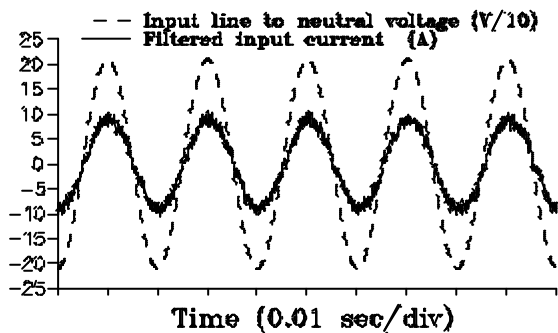


Fig.5.15 Input line-to-neutral voltage and filtered input current at 1000 rpm, 25 Nm. (reprinted from [9], Fig.12, pp.747)

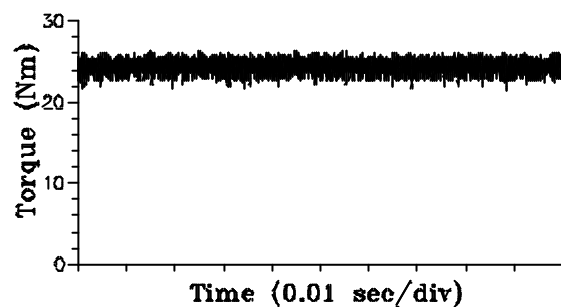


Fig.5.16 Electromagnetic torque at 1000 rpm, 25 Nm. (reprinted from [9], Fig.11, pp.747)

Afterwards the control scheme has been implemented on the 7 kVA matrix converter prototype. The experimental results showed that the input filter and the AC mains supply impedance could not be neglected in order to get realistic results for the input line currents.

For this reason, the mathematical model of Fig.5.12 has been modified in order to match the more realistic schematic circuit shown in Fig.5.17. The numerical results shown hereinafter have been obtained using this new implemented mathematical model.

Furthermore, with a comparison of the numerical and experimental results in view, the simulation parameters have been set equals to the experimental ones. Then, a cycle period of ≈ 83

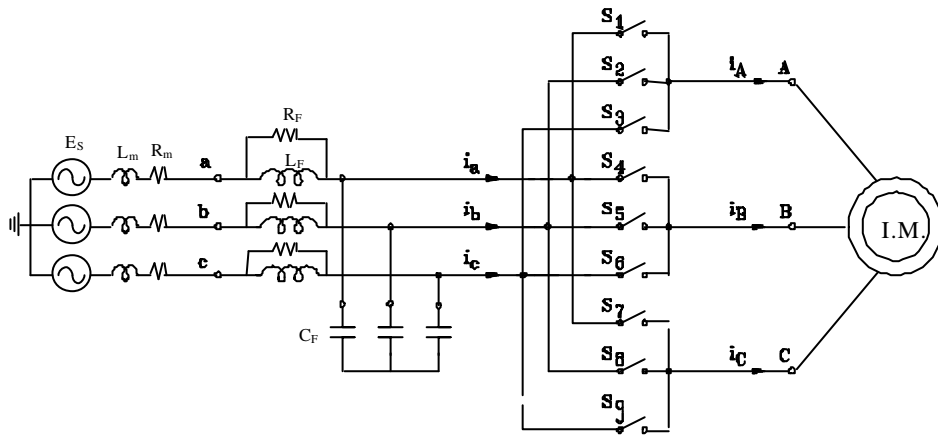


Fig.5.17 Schematic circuit of the matrix converter DTC drive.

μs , corresponding to a switching frequency of 12 kHz, has been set. The test machine data are quoted in Table IV.

Table IV.
Induction motor nameplate data and rated parameters values.

Power = 1.1 kW	Voltage = 380 V	Current = 2.7 A	Pole-pairs = 2	$\cos\phi = 0.79$
$R_S=10.21 \Omega$	$R_R=5.98 \Omega$	$L_S=0.623 \text{ H}$	$L_R=0.623 \text{ H}$	$M=0.603 \text{ H}$

For the stator flux magnitude a reference value $\phi_{S\text{ref}}$ of 0.97 Wb and an hysteresis band equal to $\pm 0.5\%$ of the reference value has been considered.

For the electromagnetic torque a reference value T_{ref} of 7.5 Nm with a hysteresis band of $\pm 10\%$ has been settled. The rotation speed of the motor was 500 rpm.

As far as the other system parameters is concerned their values are quoted in Table V with reference to the labels shown in Fig.5.17.

Table V.
AC mains and input filter parameters values.

$E_{S\text{max}}$	L_m	R_m	R_F	L_F	C_F
310 V	200 μH	0.5 Ω	37 Ω - 7 W	1.2 mH	14.8 μF

In Figs.5.18-5.23 some numerical results are shown. In Fig.5.18 the stator current is shown. As it can be seen the current waveform is sinusoidal with a high frequency ripple. The performance in terms of stator flux and electromagnetic torque are good even though not as good as in Figs.5.14 and 5.16. This is due to the doubled control cycle period, which also doubles the delay caused by the sampling of the signals.

Looking at Fig.5.22 it can be verified that the control operates in order to keep the matrix converter input current in phase with the correspondent line-to-neutral voltage. This demonstrates the validity of the proposed control method in achieving unity input power factor. In Fig.5.23 the estimated value of the average value of $\sin \psi_i$ is shown.

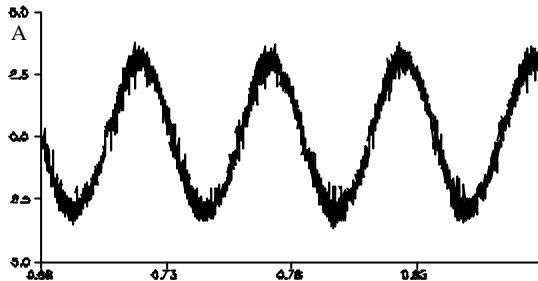


Fig.5.18 Stator current

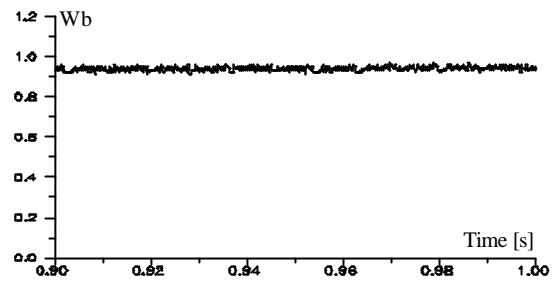


Fig.5.19 Stator flux magnitude.

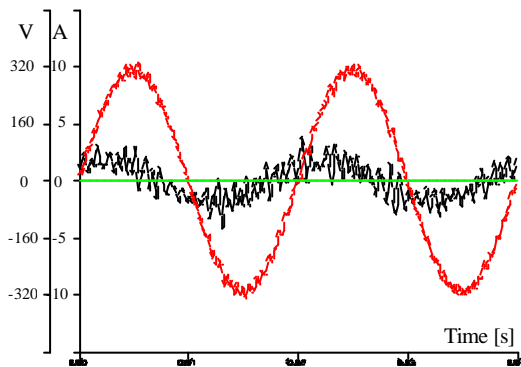


Fig.5.20 Input line-to-neutral voltage and relevant line current.

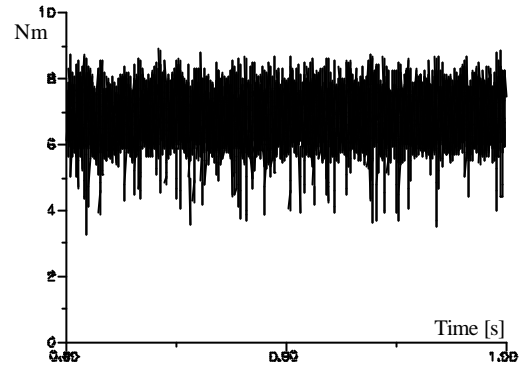


Fig.5.21 Electromagnetic torque.

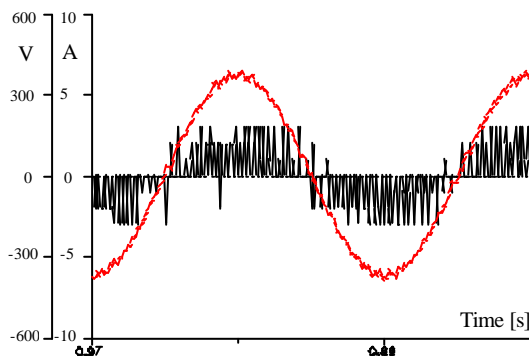


Fig.5.22 Input line-to-neutral voltage and relevant input current.

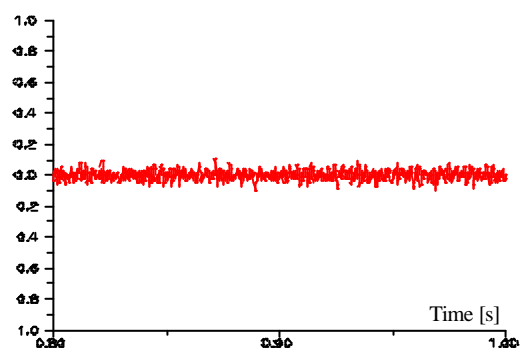


Fig.5.23 Estimated $\langle \sin \psi_i \rangle$.

Last but not least, in Fig.5.20 the input line current and the relevant input line-to-neutral voltage are shown. It can be clearly seen that the input line current has a significant harmonic distortion and is leading the voltage. The leading phase displacement is due to the input filter capacitance which is oversized with respect to the induction motor rated power for getting an unity power factor on the AC mains. Some comments about the capacitance oversizing and the line current harmonic distortion will be given in section 5.6.

5.5 Implementation of the DTC scheme and laboratory setup of the drive system

The proposed control strategy has been implemented on a 7 kVA matrix converter prototype feeding a standard three phase 1.1 kW, 4-pole, 380 V star connected, 50 Hz cage induction motor. A block diagram of the system is shown in Fig.5.24.

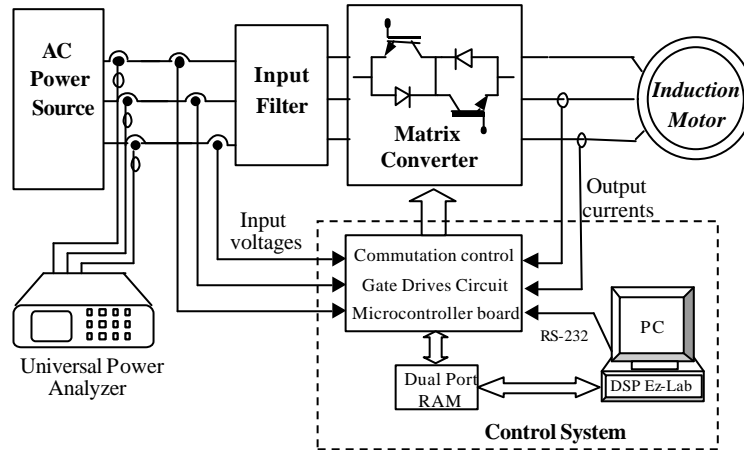


Fig.5.24 Block diagram of the laboratory Matrix-DTC drive system.

The system setup is basically the one that has been used for the SVM modulation strategies tests and that has been already described in section 4.5.2. For this reason, in this section only details on different system settings with respect to that description will be given.

The AC Power Source have been used to generate a balanced and sinusoidal three phase supply voltage system with a 310 V peak value for the line-to-neutral voltages. The line impedance was set to 0.5 Ω phase resistance and 200 μH phase inductance.

The capacitance of the LC filter have been increased despite of the lower rated load power and set to 14,8 μF . This was done to reduce the input filter cut-off frequency. In addition, in order to damp oscillations, a 37 Ω -7W resistor was applied in parallel to the filter inductances.

With regard to the control system, it is worth noting that several modifications have been brought to the micro-controller program. With respect to the SVM control, the timing of the cycle period was modified. Moreover, the program was modified in order to apply to the motor just one matrix switching configuration per cycle period.

The values of the reference control quantities were those quoted in the previous section for the numerical simulations: reference stator flux amplitude and electromagnetic torque equal to 0.97 Wb and 7.5 Nm respectively. The hysteresis band was $\pm 0.5\%$ for the stator flux and $\pm 10\%$ for the torque. Zero was the value for the reference $\langle \sin \psi_i \rangle^*$ as well as for its hysteresis band. The sampling frequency was 12 kHz ($\cong 83 \mu\text{s}$ cycle period). The motor was operated at 500 rpm approximately.

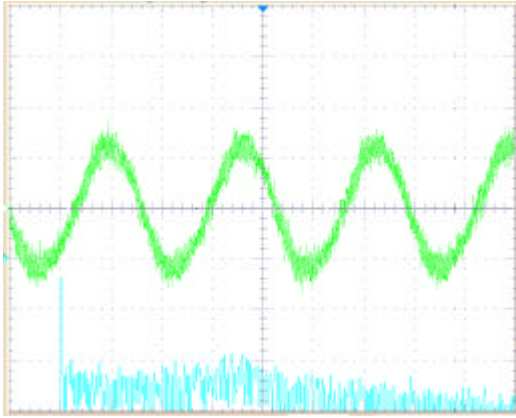


Fig.5.25 Stator current 2.5 A/div, 20 ms/div, and relevant harmonic spectrum. 20 dB/div, 625 Hz/div. $T_{ref}=7.5$ Nm.

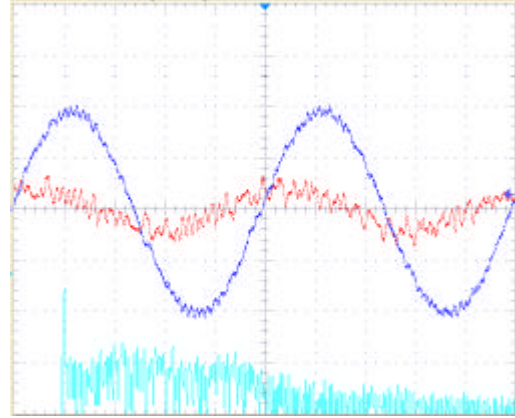


Fig.5.26 Input line-to-neutral voltage and line current, 160V/div, 5A/div, 4ms/div, with harmonic spectrum 20 dB/div, 625 Hz/div. $T_{ref}=7.5$ Nm.

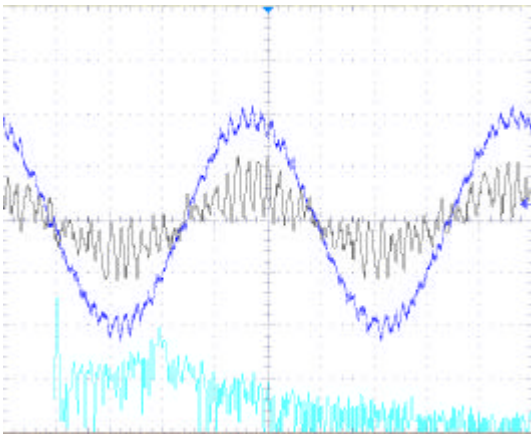


Fig.5.27 Input line-to-neutral voltage and input current, 160V/div, 5A/div, 4ms/div, with harmonic spectrum 20dB/div, 625Hz/div. $T_{ref}=15$ Nm.

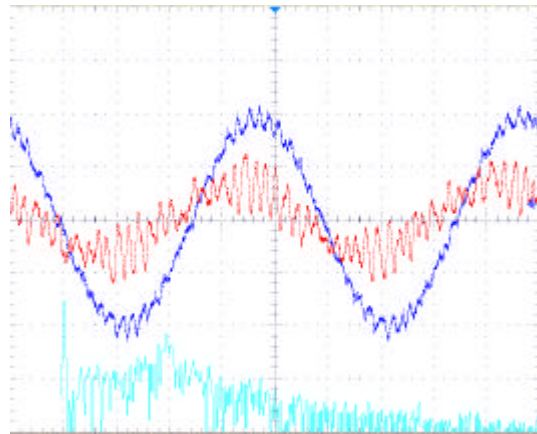


Fig.5.28 Input line-to-neutral voltage and line current, 160V/div, 5A/div, 4ms/div, with harmonic spectrum 20dB/div, 625Hz/div. $T_{ref}=15$ Nm.

In Fig.5.25 the measured stator current is shown. Its waveform is sinusoidal with a high frequency ripple, in accord with the numerical result shown in Fig.5.18. With regard to the input line current performance the simulation results hold in the practical case too, as shown by Fig.5.26.

In Figs.5.27 and 5.28 the matrix converter input current and the line current for a doubled reference torque value are respectively shown. Fig.5.27 shows that the input current is in phase with the corresponding line-to-neutral voltage, confirming that the proposed control can accomplish unity input power factor for the matrix converter. The measurement of the matrix converter input current for Fig.5.27 was carried out following the procedure afore-described in section 4.5.4. The phase displacement of the line current in Fig.5.28 is reduced by the doubled power delivered to the load, but it is evident that the harmonic distortion is increased.

In Figs.5.29 and 5.30 the stator flux magnitude and electromagnetic torque estimated by the DSP, run-time, are shown. In Tables VI and VII measurements data collected for $T_{ref}=7.5$ Nm

by the power analyzer are quoted.

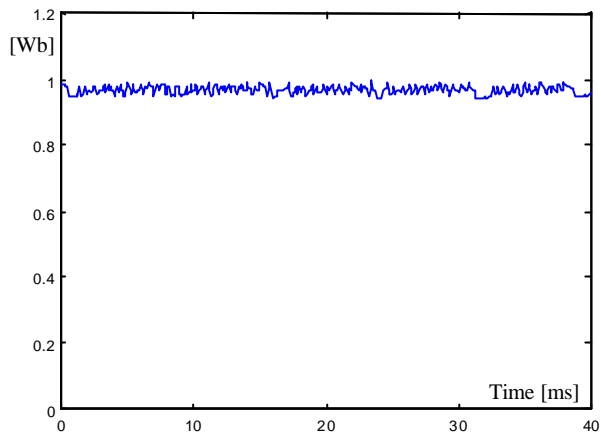


Fig.5.29 Stator flux magnitude estimated run-time by the DSP.

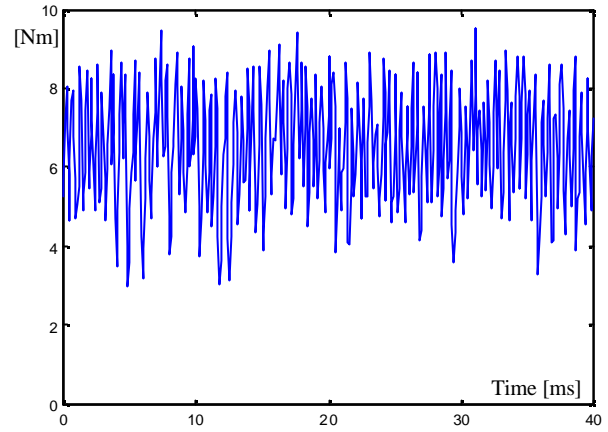


Fig.5.30 Electromagnetic torque estimated run-time by the DSP.

Table VI
Measured data for no-load conditions.

	Phase a	Phase b	Phase c
V_{rms}	220.1	220.1	220.3
I_{rms}	1.188	1.185	1.199
Watt	1	1.6	3
Var	261	260	264
$\cos\phi$	0.004	0.006	0.011
$I_{I\text{THD}}$	2	1.4	2.3

Table VII
Measured data for $T_{ref} = 7.5$ Nm.

	Phase a	Phase b	Phase c
V_{rms}	219.4	219.4	219.4
I_{rms}	1.59	1.57	1.6
Watt	188	190	192
Var	293	286	295
$\cos\phi$	0.543	0.556	0.548
$I_{I\text{THD}}$	41.9	39.1	41.4

Comparing the experimental results to the numerical ones it can be stated that there is a good accordance. This proves the validity of the implemented numerical model, which can be used for further analysis.

5.6 Input line current analysis

As it has been shown by the previous figures and by the Table VII the input line current is significantly distorted. The wide oscillations of the input line current are due to a resonance phenomenon which occurs between the AC mains line impedance and the impedance of the input current filter.

In Fig. 5.31 the complex harmonic spectrum of the input line current vector \vec{i}_s relevant to the case of Figs.5.20 and 5.26 is shown. For displaying purpose, the scale of the y axis has been truncated to 1A. It can be seen that the current harmonic components with higher amplitude are centered around the resonance frequency of the inductive-capacitive impedance of the AC main-input filter system, which is approximately 1.1 kHz.

The reasons of this resonance phenomenon are related to the control cycle period, to the DTC technique and to the matrix converter switching configuration selection table, Table III, used by the proposed control scheme.

The matrix converter cycle period used in the simulations and in the experimental tests was $\cong 83 \mu\text{sec}$. This value is higher than the cycle period values commonly used in DTC drives. Fig.5.32 clearly shows the benefits, in terms of input current distortion, of a reduced control cycle period.

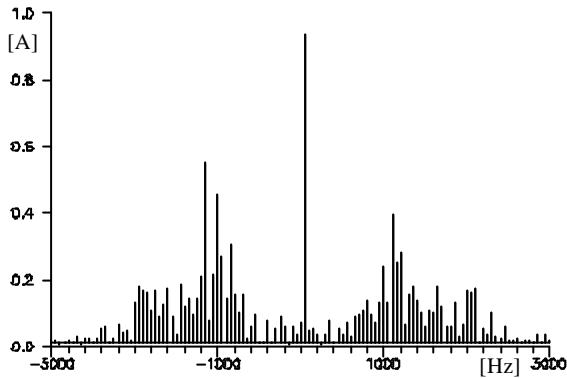


Fig.5.31 Harmonic spectrum of the input line current vector. $T_{\text{ref}}=7.5\text{Nm}$. $t_c = 83 \mu\text{s}$.

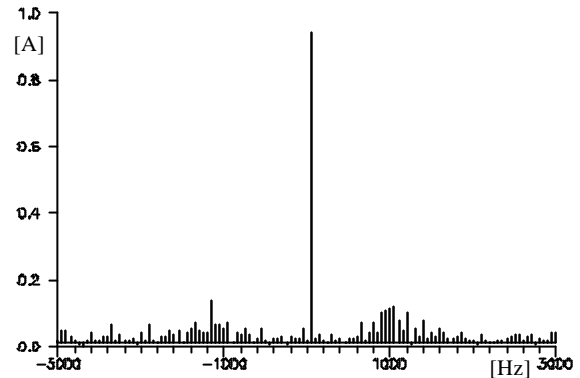


Fig.5.32 Harmonic spectrum of the input line current vector. $T_{\text{ref}}=7.5\text{Nm}$. $t_c = 40 \mu\text{s}$.

With regard to the DTC technique, a problem arises from its inherent variable switching frequency, due to the stator flux and the torque hysteresis regulators [6]-[8], [12], [13]. As a consequence, input currents and output voltages have frequency spectra which show harmonic components even at frequencies below the sampling frequency. This makes more difficult the design and the optimization of the input current filter.

As far as the matrix configuration selection algorithm is concerned it is needed to refer to Table III and Table I. Hereinafter it is rewritten the most left hand side column of Table III and the input/output features of the relevant configurations.

Table VIII.

		①												
C_ψ		+1	S.C.	A B C	v_{AB}	v_{BC}	v_{CA}	i_a	i_b	i_c	e_o	a_o	i_i	b_i
V_1	-3		+3	<i>c a a</i>	v_{ca}	0	$-v_{ca}$	$-i_A$	0	i_A	$2/3 v_{ca}$	0	$2/\sqrt{3} i_A$	$7p/6$
V_2	9		-3	<i>a c c</i>	$-v_{ca}$	0	v_{ca}	i_A	0	$-i_A$	$-2/3 v_{ca}$	0	$-2/\sqrt{3} i_A$	$7p/6$
V_3	-6		+6	<i>a c a</i>	$-v_{ca}$	v_{ca}	0	$-i_B$	0	i_B	$2/3 v_{ca}$	$2p/3$	$2/\sqrt{3} i_B$	$7p/6$
V_4	3		-6	<i>c a c</i>	v_{ca}	$-v_{ca}$	0	i_B	0	$-i_B$	$-2/3 v_{ca}$	$2p/3$	$-2/\sqrt{3} i_B$	$7p/6$
V_5	-9		+9	<i>a a c</i>	0	$-v_{ca}$	v_{ca}	$-i_C$	0	i_C	$2/3 v_{ca}$	$4p/3$	$2/\sqrt{3} i_C$	$7p/6$
V_6	6		-9	<i>c c a</i>	0	v_{ca}	$-v_{ca}$	i_C	0	$-i_C$	$-2/3 v_{ca}$	$4p/3$	$-2/\sqrt{3} i_C$	$7p/6$

Table IX.

		①												
C_ψ	-1		S.C.	A B C	v_{AB}	v_{BC}	v_{CA}	i_a	i_b	i_c	e_o	a_o	i_i	b_i
V_1	1	+1	a b b	v_{ab}	0	$-v_{ab}$	i_A	$-i_A$	0	$2/3 v_{ca}$	0	$2/\sqrt{3} i_A$	$7p/6$	
V_2	-7	-1	b a a	$-v_{ab}$	0	v_{ab}	$-i_A$	i_A	0	$-2/3 v_{ca}$	0	$-2/\sqrt{3} i_A$	$7p/6$	
V_3	4	+4	b a b	$-v_{ab}$	v_{ab}	0	i_B	$-i_B$	0	$2/3 v_{ca}$	$2p/3$	$2/\sqrt{3} i_B$	$7p/6$	
V_4	-1	-4	a b a	v_{ab}	$-v_{ab}$	0	$-i_B$	i_B	0	$-2/3 v_{ca}$	$2p/3$	$-2/\sqrt{3} i_B$	$7p/6$	
V_5	7	+7	b b a	0	$-v_{ab}$	v_{ab}	i_C	$-i_C$	0	$2/3 v_{ca}$	$4p/3$	$2/\sqrt{3} i_C$	$7p/6$	
V_6	-4	-7	a a b	0	v_{ab}	$-v_{ab}$	$-i_C$	i_C	0	$-2/3 v_{ca}$	$4p/3$	$-2/\sqrt{3} i_C$	$7p/6$	

Before to proceed it is important to remind that only a switching configuration per cycle period is applied to the matrix converter and such configuration changes only when the output signal of one of the three hysteresis comparators changes or the input current vector changes its sector.

Bearing in mind these remarks Table VIII is considered. Table VIII shows that when vector \vec{i}_i is in sector ① and the hysteresis comparator C_ψ is equal to +1, all the switching configurations quoted in the relevant column keep to zero the same matrix converter input current, which in the case is i_b . In the same way, all the switching configurations quoted in the column of C_ψ equal to -1, Table IX, keep to zero the input current i_c . The same happens for the other sectors of \vec{i}_i .

What does this imply?

This means that for a given sector of \vec{i}_i , whose value does not vary for 1/6 of the fundamental period, and a given value of the hysteresis regulator C_ψ , whose rate of change depends on the time constant of the $\sin \psi_i$ low pass filter, whatever vector is required by the DTC control, the correspondent matrix converter configuration keeps to zero the same converter input current. The effect is a further reduction of the input currents switching frequency which leads to the appearance of significant current harmonic components even around the resonance frequency of the input filter-AC mains impedance system.

How this harmonic distortion might be reduced?

Looking at Tables VIII and IX, it can be noted that the matrix switching configurations which, for sector ① of \vec{i}_i , are listed in different columns of C_ψ , keep to zero different converter input phase currents. It can be verified by Tables I and III that this rule holds for any sector of the \vec{i}_i vector.

It is then of interest to give a glance to the $\langle \sin \psi_i \rangle$ control variable by whom the signal C_ψ depends on. In the numerical simulations as well as in the prototype DSP implemented control program, a first order digital filter truncated at the second order was used in order to obtained $\langle \sin \psi_i \rangle$. This digital filter is equivalent to a low pass filter whose cut off frequency depends on the filter time constant. Higher the time constant lower the cut off frequency. In other words,

setting a high value for the digital filter time constant the responsiveness of the filter to the instantaneous variation of $\sin \psi_i$ is reduced and consequently the signal C_ψ has a minor rate of change.

On the basis of these considerations some improvements might be expected decreasing the time constant of the digital filter in order to increase the rate of change of C_ψ . In this way, a more frequent switching between the two columns of the current sector of \bar{i}_i will occur, yielding an increase of the converter input currents switching frequency. The results obtained by the experimental tests have met such expectation. Decreasing the digital filter time constant a reduction of the input line current total harmonic distortion (THD) was obtained. Yet, the time constant can not be decreased indefinitely, because below a certain value the filter does no longer carry out the needed filtering action.

5.7 Modified control method for improving the input line current

On the basis of the previous input line current analysis, a modified control method has been implemented and verified by means of numerical simulations. This control method allows to reduce the harmonic content of the input line current without any negative effect on the drive performance and its control simplicity.

The basic principle is to use, within a cycle period, both the switching configurations that the matrix converter provides to the classical DTC scheme.

Instead of choosing one of these two configurations, accordingly to the hysteresis comparator output signal C_ψ , both the configurations are applied but for different time intervals, in such a way that, in a cycle period, the average effect on the converter input current vector is that required by C_ψ . The improvement obtained with this solution is due to the fact that the two configurations keep to zero different converter input currents along with an increase of the matrix converter switching frequency.

The following example is given to explain the modified control method. The cycle period is still 83 μsec .

It is assumed that the DTC scheme represented by Table II requires the application of vector \bar{V}_1 , the vector \bar{i}_i is in sector **1** and the input power factor hysteresis comparator sets $C_\psi = +1$. The original control, accordingly to Table III, would apply the switching configuration -3 for the whole cycle period t_C . The modified control will apply both the switching configurations -3 and +1, for a time period t_{-3} and t_{+1} respectively, where

$$t_{-3} = \alpha_I \cdot t_C \quad (5.10)$$

$$t_{+1} = \alpha_{II} \cdot t_C \quad \text{with} \quad \alpha_I > \alpha_{II} \quad (5.11)$$

and a_I and a_{II} are constants whose optimum values have been determined by a trial and error method.

In this way, within a cycle period, the average effect on the converter input current vector displacement angle is that required by C_{ψ} . In Fig.5.33 the harmonic spectrum of the input line current vector for the modified control strategy is shown. The operating conditions are the same of Fig.5.31.

It can be seen that the modified control strategy allows a reduction of the higher amplitude harmonic components. With regard to the stator flux and the electromagnetic torque, the modified control method preserves the good performance of the original one, as it can be seen from Fig.5.34 and 5.35. From an implementation point of view, the modified control method needs only few additional calculations.

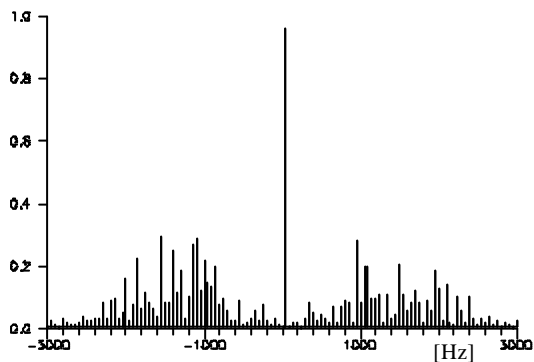


Fig.5.33 Harmonic spectrum of the input line current Modified control strategy.

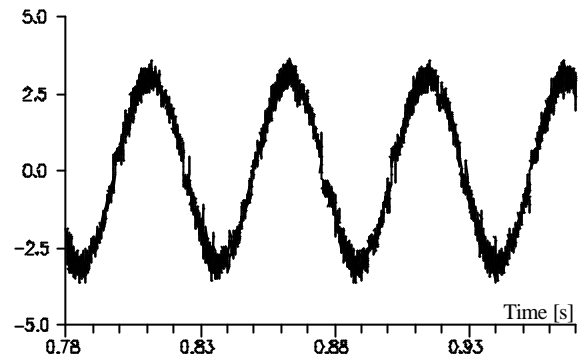


Fig.5.34 Stator current. Modified control strategy.

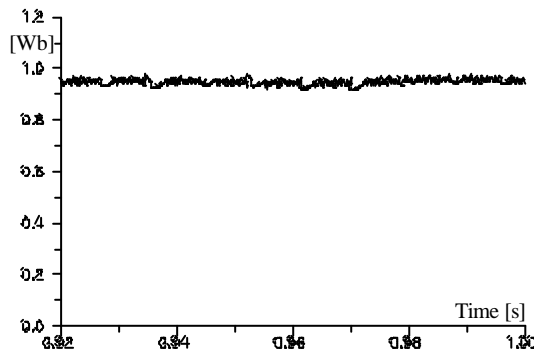


Fig.5.35 Stator flux magnitude. Modified control strategy.

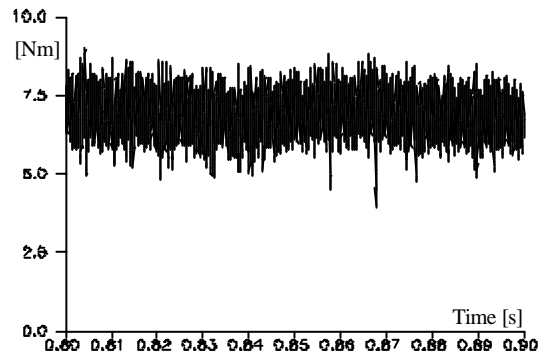


Fig.5.36 Electromagnetic torque. Modified control strategy.

5.8 Conclusions

In this chapter a control method based on classical direct torque control technique has been presented for a matrix converter induction motor drive.

The control method is based on switching tables which allows the direct control of the matrix converter accordingly to the motor and input power factor requirements. By means of this new control method the advantages of matrix converters over traditional VSI-PWM converters, such as unity power factor control, inherent bi-directional power flow and sinusoidal input current capability, have been combined with the control simplicity and robustness of the DTC technique.

At any cycle period, the opportune matrix converter switching configuration to apply is selected entering the switching table by the outputs of three hysteresis controllers applied to the errors of stator flux, electromagnetic torque and input power factor, respectively.

The performance of the control scheme have been analyzed both by numerical simulations and experimental tests. The analysis has shown that the proposed control scheme can provide good performance for the induction motor and unity input power factor but the input line current can be significantly distorted if the sampling frequency is not sufficiently high.

In fact, due to the inherent variable switching frequency of the DTC scheme and to the features of control switching table, the input current can have harmonic components at frequency much below the sampling frequency which can excite resonance phenomena of the AC mains impedance and input current LC filter.

On the basis of the analysis carried out a modified control scheme which improves the input line current quality without negatively affecting the drive performance has been presented and verified by numerical simulations.

References

- [1] I.Takahashi, T. Noguchi, "A new quick-response and high-efficiency control of an induction motor," IEEE Transactions on Industry Applications, Vol. IA-22,N. 5, Sept./Oct. 1986, pp. 820-827.
- [2] M. Depenbrok, "Direct Self-Control (DSC) of Inverter-Fed Induction Machine," IEEE Transactions on Power Electronics, Vol. PE-3,N. 4, Oct. 1988, pp. 420-429.
- [3] I.Takahashi, T. Noguchi, "Ultra-Wide speed control with a quick torque response AC servo by a DSP," Proceedings EPE'91, Firenze, Italy, Vol. 3, pp. 572-577.
- [4] I. Boldea and S.A. Nasar, "Torque Vector Control (TVC) - A Class of Fast and Robust Torque Speed and Position Digital Controller for Electric Drives," Proceedings of EMPS, vol. 15, 1988, pp. 135-148.
- [5] J.N. Nash, "Direct Torque Control, Induction Motor Vector Control Without an Encoder", IEEE Transactions on Industry Applications, Vol. 33, N. 2, March/April 1997, pp. 333-341

- [6] D. Casadei, G. Grandi, G. Serra, A. Tani "Effects of flux and torque hysteresis band amplitude in direct torque control of induction machines," Proceedings of IECON'94, 5-9 September 1994, Bologna, Italy, pp. 299-304.
- [7] D. Casadei, G. Grandi, G. Serra, A. Tani "Switching strategies in direct torque control of induction machine," Proceedings of ICEM'94, Paris, France, 5-8 September 1994, pp. 204-209
- [8] Ch. Lochot, X. Roboam, P. Maussion, "A new direct torque control strategy for an induction motor with constant switching frequency operation," Proceedings of EPE'95, Sevilla, Spain, pp. 2431-2436.
- [9] D. Casadei, G. Grandi, G. Serra, A. Tani "The use of matrix converters in direct torque control of induction machines," Proceedings of IECON'98, Aachen, Germany, August 31-September 4, 1998, pp. 744-749.
- [10] F. Blaabjerg, D. Casadei, M. Matteini, G. Serra, A. Tani, "Direct Torque Control using Matrix Converters: Improvement of the Input Line Current Quality," Proceedings of EPE 2001, Graz, Austria, 27-29 August, 2001, CD-ROM, pp. 1-10, 2001.
- [11] H. Bausch, R. Blumel, W. Zeng, "Flux-Estimation of a PWM-Inverter-Fed Torque-Controlled Induction Machine based on Terminal Quantities," Proceedings of ICEM'92, Manchester (UK), September 15-17 1992, pp. 833-837.
- [12] D. Casadei, G. Serra, A. Tani, "Performance Analysis of a DTC control scheme for Induction Motor in the low speed range", Proceedings of EPE'97, Trondheim, Norway, 8-10 September 1997, Vol. 3, pp. 700-704, 1997.
- [13] I. Ludtke, M. G. Jayne, "A comparative study of high performance speed control strategies for voltage-sourced PWM inverter-fed induction motor drives," Proceedings of EMD'95, Durham, UK, 11-13 September, 1995, pp. 343-348, 1995.